Carbohydrate Polymers 167 (2017) 167–176

Contents lists available at ScienceDirect

Carbohydrate Polymers

journal homepage: www.elsevier.com/locate/carbpol

Integrated production of lignin containing cellulose nanocrystals (LCNC) and nanofibrils (LCNF) using an easily recyclable di-carboxylic acid

Huiyang Bian[a,c], Liheng Chen[b,c], Hongqi Dai[a], J.Y. Zhu[c,*]

[a] Jiangsu Provincial Key Lab of Pulp and Paper Science and Technology, Nanjing Forestry University, Nanjing 210037, China
[b] Key Laboratory of Biomaterials of Guangdong Higher Education Institutes, Department of Biomedical Engineering, Jinan University, Guangzhou 510632, China
[c] Forest Products Laboratory, U.S. Forest Service, U.S. Department of Agriculture, Madison, WI 53726, USA

ARTICLE INFO

Article history:
Received 21 December 2016
Received in revised form 3 March 2017
Accepted 14 March 2017
Available online 18 March 2017

Keywords:
Lignin containing cellulose nanomaterials
Lignocellulosic crystals (LCNC)
Lignocellulosic nanofibrils (LCNF)
Di-carboxylic acid hydrolysis
Mechanical fibrillation
Thermal stability
Carboxylation
Hydrophobicity

ABSTRACT

Here we demonstrate di-carboxylic acid hydrolysis for the integrated production of lignin containing cellulose nanocrystals (LCNC) and nanofibrils (LCNF) using two unbleached mixed hardwood chemical pulps of lignin contents of 3.9 and 17.2%. Acid hydrolysis experiments used maleic acid solution of 60 wt% concentration at 120 °C for 120 min under ambient pressure. Yields of LCNC were low of less than 6% under this set of conditions. The higher lignin content sample produced LCNC with greater height (diameter) of 25 nm but similar length of approximately 230 nm to that from the lower lignin content fibers (height of 20 nm). Interestingly, the higher lignin content sample resulted in LCNF with smaller height (diameter) of 7 nm but longer length of >1 μm, or greater aspect ratio than the LCNF from the lower lignin fibers of height 10 nm and length <1 μm. Lignin protected cellulose from esterification which resulted in LCNC and LCNF that was less carboxylated compared to those lignin-free CNC and CNF and therefore had lower charges. However, lignin is more hydrophobic and thermally stable than carbohydrates therefore LCNC and LCNF are favorable for composite applications.

Published by Elsevier Ltd.

1. Introduction

Cellulose nanofibrils (CNF) and nanocrystals (CNC) derived from various cellulose sources have gained much attention as a green alternative for applications in composites, packaging materials, and electronics (Eichhorn et al., 2010; Rojo et al., 2015; Zhu et al., 2016). CNF are produced through pure mechanical fibrillation (Hoeger et al., 2013; Iwamoto, Nakagaito, & Yano, 2007; Wang, Zhu, Gleisner, et al., 2012), or by chemical or enzymatic pretreatment followed by mechanical fibrillation to reduce energy cost in fibrillation (Chen, Zhu, Baez, Kitin, & Elder, 2016; Li, Sirviö, Haapala, & Liimatainen, 2017; Qin, Qiu, & Zhu, 2016; Saito, Okita, Nge, Sugiyama, & Isogai, 2006; Sehaqui et al., 2017; Siró et al., 2011; Wang et al., 2015). CNC are commonly produced using mineral acid hydrolysis (Chen et al., 2015; Hamad & Hu, 2010). Recently solid di-carboxylic acids were also used which solved the problem of acid recovery and achieved integrated production of thermally stable and carboxylated CNC with CNF from bleached chemical pulp fibers (Chen et al., 2016; Wang, Chen, Zhu, & Yang, 2017). Integrated production of CNF with CNC was first reported by the present authors using sulfuric acid hydrolysis of bleached pulp fibers in producing CNC at low severities through subsequent mechanical fibrillation of partially hydrolyzed non-CNC cellulosic solids residue (CSR) into CNF (Wang, Zhu, & Considine, 2013; Wang, Zhu, Reiner et al., 2012). Later, researchers demonstrated the production of CNC from CNF through further chemical reactions by the removal of disordered cellulose (Peyre, Pääkkönen, Reza, & Kontturi, 2015; Usov et al., 2015).

So far, most research work on cellulose nanomaterial production, especially CNC, used lignin-free (fully-bleached) chemical pulp fibers. Lignin, composed of different kinds of phenylpropane units, is considered to be the glue (middle lamella lignin) that holds together other major biopolymers in plant biomass (Ferrer et al., 2012). Lignin is also more thermally stable than cellulose or hemicelluloses. Its inclusion in cellulose nanomaterials provides improved thermal stability (Poletto, Zattera, Forte, & Santana, 2012). Moreover, lignin (inside cell wall) can be used to adjust the polarity and hydrophilicity of cellulose (Poletto et al., 2012).

* Corresponding author.
E-mail address: jzhu@fs.fed.us (J.Y. Zhu).

http://dx.doi.org/10.1016/j.carbpol.2017.03.050
0144-8617/Published by Elsevier Ltd.

Therefore, using lignin-containing cellulosic fibers for producing cellulose nanomaterials is expected to generate more hydrophobicity, allowing improved dispersion in non-polar media, and in particular, when forming composites with typical hydrophobic matrices (Spence, Venditti, Rojas, Habibi, & Pawlak, 2010). Furthermore, using unbleached pulp as an alternative feedstock can produce lignin containing cellulose nanomaterials at higher yields and lower costs compared with using bleached pulp (Rojo et al., 2015).

There are no publicly available studies on the production of lignin containing cellulose nanocrystals (LCNC). Only a few studies have reported on the production of lignin containing cellulose nanofibrils (LCNF) using pure mechanical fibrillation of unbleached chemical pulp fibers (Rojo et al., 2015; Spence, Venditti, Habibi, Rojas, & Pawlak, 2010). Studies using low lignin content fibers suggested insignificant effects from lignin on LCNF thermal and water absorption properties (Chen et al., 2011). Improved water interaction and fibrillation, however, were found with fibers containing lignin at a moderate level of 13% (Ferrer et al., 2012; Spence, Venditti, Rojas et al., 2010). When using undelignifed wood fibers with lignin contents >25%, microfibrillation became very difficult (Hoeger et al., 2013; Spence, Venditti, Habibi et al., 2010). Recently, a comprehensive study was carried out using laboratory pulp fibers containing up to 13.5 wt% lignin produced using a noncommercial SO_2-ethanol solvent process (Rojo et al., 2015). The study concluded that lignin did not reduce mechnical strength of films made of the resultant LCNF, as the lignin did not interfere with hydrogen bonding. Lignin substantially changed the interfacial free energy and increased hydrophobicity. However, the lignin contained in this laboratory pulp sample was slightly sulfonated, due to the pulping process using large amounts of SO_2, and therefore the fibers were relatively less hydrophobic or slightly more hydrophilic. As a result, the pulp fibers and the resultant cellulose nanomaterials may behave differently from conventional commercial kraft pulp fibers (with highly hydrophobic lignin). Furthermore, existing LCNF stuides all used pure mechanical fibrillation which is energy intensive especially for fibers with high lignin content (Hoeger et al., 2013; Rojo et al., 2015; Spence, Venditti, Rojas, Habibi, & Pawlak, 2011; Wang, Zhu, Gleisner et al., 2012). Moreover, the resultant LCNF has low surface charges and contains only a very small amount of functional groups originating from the feed fibers, which makes dispersion and surface modification difficult in downstream processing.

Here we use a concentrated solid di-carboxylated acid to hydrolyze hemicelluloses and depolymerize cellulose to achieve integrated production of LCNC and LCNF from two commercial unbleached kraft mixed hardwood pulps with lignin contents of 3.9 and 17.2%, respectively. As weak acids, di-carboxylic acids cannot depolymerize all the pulp fibers to LCNC. The remaining lignocellulosic solid residue (LCSR) is partially hydrolyzed fibers which can be subsequently fibrillated to LCNF. Acid hydrolysis can substantially reduce energy requirements in mechanical fibrillation (Qin et al., 2016; Wang et al., 2013; Wang, Zhu, Reiner et al., 2012). Furthermore, concentrated di-carboxylated acids can esterifiy cellulose (Fischer & Speier, 1895) to result in a carboxylated cellulosic material (Allen & Cuculo, 1973), as demonstrated previously (Chen et al., 2016), which is important to downstream processing for a variety of applications. Moreover, solid di-carboxylic acids are environmentally benign and can be easily recovered simply through commercially proven crystalliztaion processes (Chen et al., 2016). The significance of the work lies in its potential for low cost and environmentally sustainable integrated production of LCNC and LCNF compared with existing chemcial pretreatment methods such as oxidation (Liimatainen, Visanko, Sirviö, Hormi, & Niinimaki, 2012; Saito et al., 2006) or mineral acid hydrolysis. We are not aware of similar studies being reported in the public litearture.

2. Materials and methods

2.1. Materials

Anhydrous maleic acid was purchased from Sigma-Aldrich (St. Louis, MO). Bleached eucalyptus kraft dry lap pulp (BEP) was obtained from Aracruz Cellulose (Brazil). Two unbleached never dried virgin mixed hardwood (mainly birch and maple) kraft pulps (in suspension) with high (UHP-LL) and low (UHP-HL) lignin contents, or kappa numbers, were complimentarily provided by the International Paper Company (Loveland, OH). These two pulp samples were acquired from the same mill (Cantonment, FL) at the same day but different production lines (liner board pulp of high kappa and fluff pulp of low kappa). They are expected to have the same wood species mix. The fibers of these two pulp samples have an average length and diameter of approximately 2 mm and 30 μm, respectively, compared with approximately 1.0 mm and 25 μm for those of BEP fibers (Fig. 1a–c). The main chemical compositions were analyzed by the Analytical Chemistry and Microscopy Laboratory (ACML) at the US Forest Service, Forest Products Laboratory. Wiley-milled samples were hydrolyzed using sulfuric acid in two steps as described previously (Luo et al., 2010). The solubilized carbohydrates in the hydrolysates were analyzed using ion chromatography with pulsed amperometric detection. Klason lignin was determined gravimetrically. The kappa number of the pulps were measured according to TAPPI Standard Method T236 om-99 (TAPPI, 1999).

2.2. Production of lignocellulosic nanocrystals and nanofibrils

The BEP was first dispersed in de-ionized (DI) water overnight and then disintegrated using a laboratory disintegrator (TMI, Ronkonkoma, NY) at 2 wt% for 10,000 revolutions. All wet pulps were air dried to approximately 7% moisture content then stored in plastic bags. Acid hydrolyses were conducted on the pulps using 10 g oven dry (OD) fibers in a 60 wt% concentration maleic acid solution at 120 °C for 120 min, abbreviated as M60T120t120, using a liquor to fiber ratio of 10:1 (L/kg). The pulp suspensions were constantly mixed using a mechanical stirrer at 300 rpm during hydrolyses. The reactions were quenched by adding 200 mL of DI water to the suspensions at the end of each reaction. The suspension was washed and repeatedly centrifuged at 10,000 rpm for 10 min to discard the supernatant to remove acid and then dialyzed for a week or until the pH of the dialysis water no longer changed. Lignocellulosic nanocrystals (LCNC) were finally obtained by centrifuging the dialyzed solid suspension at 10,000 rpm for 10 min. The turbid supernatant suggests the presence of LCNC. The precipitated solids is partially hydrolzyed LCSR. LCNC yield was determined by a chemical oxygen demand (COD) method using a COD kit (Biosciences, Inc., Bethlehem, PA, ISO 9001:2000 certified) (Wang, Zhu, Reiner et al., 2012). COD was measured from the amount of chromium consumed determined by colorimetry at 600 nm. Assuming all COD was contributed by cellulose in quantifying LCNC through calibration. Errors were inevitably introduced due to the presence of lignin, hemicelluloses.

The LCSR was mechanically fibrillated at approximately 1% solids consistency using a microfluidizer (M-110EH, Microfluidics Corp., Westwood, MA) at an operating pressure of 120 MPa for 5 passes through two chambers in a series of diameters of 200 and 87 μm.

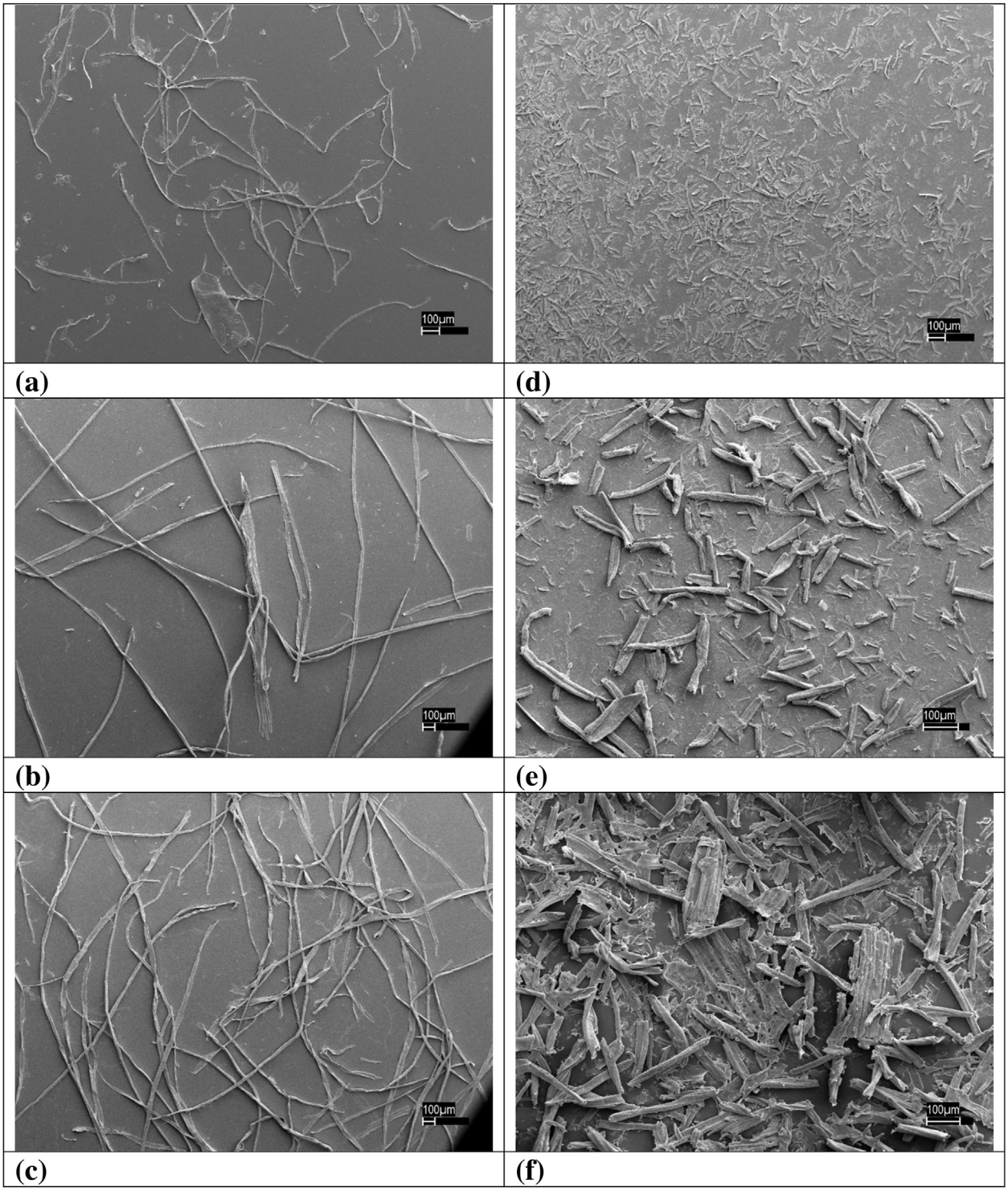

Fig. 1. SEM images of feed fibers (left panel) and lignocellulosic solid residues (LCSR) (right panel) after separating CNC from the hydrolyzed water insoluble solids (WIS). Scale bar = 100 μm. (a)-(c) BEP, UHP-LL, and UHP-HL, respectively; (d)-(f) the corresponding LCSR.

2.3. Morphology analyses

The morphologies of the LCSR samples were observed using scanning electron microscopy (SEM). Samples were prepared by drying a small amount of suspension on a well-polished aluminum mount and sputter-coating with a thin gold layer to provide adequate conductivity. Sample images were recorded using a Leo EVO 40 SEM.

The morphologies of LCNC and LCNF samples were also observed using atomic force microscopy (CS-3230, AFM workshop, Signal Hill, CA, USA). Samples were diluted to solids consistency of 0.01 wt% and deposited onto clean mica substrates and air dried overnight at room temperature. A silicon cantilever was used to image samples in vibrating tapping mode at 160–225 kHz with a radius of the tip curvature of less than 10 nm. Fibril heights and number averaged lengths were measured using Gwyddion (Department of Nanometrology, Czech Metrology Institute, Crezh

Republic, 64-bit) and Image-Pro Plus software (Media Cybernetics, Inc., Rockville, MD), respectively.

2.4. Water retention values

The water retention value (WRV) represents the total water in the pores of a substrate which closely correlates to the total pore volume (Luo & Zhu, 2011). The LCNC and LCNF are not single elementary crystals or fibrils of 3 nm in diameter rather aggregates with diameters greater than 7 nm and therefore have pores. The WRV of all substrates were measured following the standard test method SCAN-C 62:00 (SCAN, 2000). As described in our previous study (Luo & Zhu, 2011), a wet fibrous material was wrapped by a nylon screen with mesh opening of 100 μm (Cole-Parmer, Vernon Hills, IL) and placed into a centrifuge tube with support to leave space for water accumulation at the bottom of the tube during centrifuging. The wrapped sample was centrifuged at 3000 g for 15 min in a laboratory centrifuge (Thermo Fisher Scientific, Sorvall Legend 40/40R, Waltham, MA). The centrifuged sample was first weighed, then oven dried at 105 °C overnight and weighed again. The WRV is simply the percentage of retained water (weight change of the sample before and after drying) to the dried sample.

2.5. Crystallinity index

The X-ray diffraction (XRD) patterns were measured using wide-angle X-ray diffraction on a Bruker D8 130 Discover system with Cu-Kα radiation (Bruker Corp., Billerica, MA, USA) in the 2 range of 10 ~ 38° in steps of 0.02° as described previously (Chen et al., 2015). For analysis purposes, the LCNF samples were first freeze-dried and then pressed into pellets at 180 MPa. The crystallinity index (CrI) was calculated according to the Segal method (without base line subtraction) (Segal, Creely, Martin, & Conrad, 1959).

2.6. Carboxyl group content and surface charge

The carboxyl group contents of LCNC and LCNF were determined using conductometric titration. A suspension containing 50 mg LCNF was mixed with 100 mL of 1 mM NaCl solution. The mixture was then titrated with 10 mM NaOH and while its conductance was measured (YSI Model 35, Yellow Springs Instrument Co., Ohio, USA). The lowest points of the conductivity curves correspond to complete neutralization of the carboxyl groups.

The surface charge of the LCNF samples was measured using a zeta potential analyzer (Nanobrook Omni, Brookhaven Instruments, Holtsville, NY) at ambient temperature. The concentration of the suspensions was approximately 0.5 g/L. Five measurements were carried out for each sample and the averages were reported.

2.7. Fourier transform infrared spectroscopy (FTIR)

A commercial Fourier-transform infrared spectrometer (FTIR) (Spectrum Two, PerkinElmer, UK) with a universal attenuated-total-reflection (ATR) probe was used to identify ester groups in LCNF samples, as well as in the original BEP, UHP-LL and UHP-HL fibers. All samples were freeze-dried before analyses.

2.8. Thermogravimetric analysis (TGA)

Thermogravimetric analyses (TGA) of different LCNF samples were carried out on a thermogravimetric analyzer (Pyris 1, PerkinElmer, Inc., Waltham, MA). Samples of approximately 5 mg were heated from ambient to 600 °C under a 20 mL/min high purity nitrogen stream using a heating rate of 10 °C/min.

Table 1
Sample chemical compositions and component yields (in the parentheses), yields of water insoluble solids (WIS), lignocellulosic solid residues (LCSR), and lignocellulosic nanocrystals (LCNC) from maleic acid hydrolysis of different pulp fibers under acid concentration 60 wt% at 120 °C for 120 min. All yields are reported based on original fiber mass.

Sample label	Glucan (%)	Xylan (%)	Mannan (%)	Galactan (%)	Arabanan (%)	K Lignin (%); Kappa No.	WIS yield (%)	LCSR yield (%)	LCNC yield (%)
BEP	77.1 ± 1.41	15.55 ± 0.07	ND	ND	ND	0.10 ± 0.10	100		
UHP-LL	72.87 ± 1.77	7.37 ± 0.55	7.81 ± 0.06	0.74 ± 0.19	0.74 ± 0.19	3.85 ± 0.35; 23.2 ± 0.2	100		
UHP-HL	61.08 ± 1.73	8.83 ± 0.10	6.10 ± 0.37	1.37 ± 0.13	1.37 ± 0.13	17.17 ± 0.62; 90.6 ± 2.3	100		
BEP-M60T120t120	77.99 (95.2)	9.42 (57.0)	ND	ND	ND	0.43	94.16	84.27	3.02
UHP-LL-M60T120t120	75.05 (97.0)	5.24 (66.9)	6.43 (77.6)	0.37 (47.1)	0.29 (36.9)	4.59 (112.3)	94.20	84.04	5.94
UHP-HL-M60T120t120	63.37 (96.4)	5.88 (61.9)	5.03 (76.6)	0.38 (25.8)	0.86 (58.3)	18.02 (97.5)	92.89	89.94	2.10

Table 2
List of morphological, physical, chemical, and thermal properties of the BEP, UHP-LL, UHP-HL fibers and their corresponding LCNC and LCNF.

Sample Abbreviation	K. Lignin (%)	Average length (nm)	Average height (nm)	WRV (%)	CrI (%)	COOH (mmol/g)	Zeta potential (mV)	T_{onset} (°C)	T_{max} (°C)
BEP	0.1			99	76.0 ± 0.40			311	391
CNC-BEP		329.9	15.9			0.368	−46.88 ± 1.03		
CNF-BEP			13.4	1338	80.3 ± 0.34	0.059	−45.20 ± 1.96	296	361
UHP-LL	3.9			88	71.4 ± 0.34			315	410
LCNC-UHP-LL		232.9	20.7			0.235	−42.01 ± 0.83		
LCNF-UHP-LL			9.6	527	76.2 ± 0.33	0.021	−41.67 ± 1.92	320	376
UHP-HL	17.2			64	66.6 ± 0.95			325	411
LCNC-UHP-HL		236.3	25.0			0.273	−36.28 ± 1.05		
LCNF-UHP-HL			7.1	387	69.0 ± 0.61	ND	−30.96 ± 1.06	301	393

3. Results and discussion

3.1. Yields from acid hydrolysis

The water insoluble solids (WIS) from acid hydrolysis were separated through filtration and washed coupled with centrifugation. WIS yield was high of over 90%, as listed in Table 1. For comparison purpose the results from BEP were also presented. The LCNC was separated from the hydrolyzed WIS through dialysis. The remaining LCSR were retained for LCNF production through subsequent mechanical fibrillation. The yield of LCSR and LCNC were also measured after dialysis. LCNC yield was low at only a few percent since maleic acid is a weak acid and incapable of sufficiently depolymerizing chemical pulp fibers. Considering that the market for LCNC is often much smaller than that for LCNF, the present process should work well to meet market needs of these two types of cellulose nanomaterials. After the maleic acid treatment, most of the fibers end-up as partially hydrolyzed solid residue, or LCSR. Due to cellulose depolymerization (Qin et al., 2016; Wang et al., 2017), the LCSR were substantially shortened compared with the feed fibers (Fig. 1) and have lengths of approximately 100–200 μm. The fiber shortening was less pronounced for UHP than BEP due to the presence of lignin that protected against carbohydrate degradation (Wang, Zhu, Zalesny, & Chen, 2012), especially for UHP-HL with higher lignin content.

The chemical composition of the hydrolyzed WIS are also presented in Table 1. Cellulose losses were minimal at 5% or less for all the samples. Approximately 40% of the xylan were dissolved. For the two UHP samples, approximately 25% of the mannan were also dissolved. Overall, acid hydrolysis slightly enriched cellulose content in the WIS.

3.2. Morphologies of LCNC and LCNF

AFM images of the CNC from BEP, and LCNC from UHP-LL and UHP-HL indicate good dispersion as shown in Fig. 2. The lengths of the LCNC samples from the two unbleached pulps were approximately the same (Table 2). Lignin particles were clearly visible in both of these samples. CNC particles from BEP appear less uniform in terms of length than those from the unbleached mixed hardwood pulp of UHP-LL and UHP-HL (comparing Fig. 2a with Fig. 2b and c). Height measurements by AFM indicate that high lignin content resulted in crystals with greater height (right panels in Fig. 2), suggesting that lignin protected against cellulose depolymerization to result in crystals with larger diameters. The number averaged height for the CNC-BEP and LCNC-UHP-LL and LCNC-UHP HL were 15.9, 20.7, and 25.0 nm (Table 2), respectively.

The three LCSR samples from acid hydrolysis of BEP, UHP-LL, and UHP-HL under the same condition were subsequently fibrillated into LCNF in the form of sol gels as shown in the left panel of Fig. 3. AFM topography measured fibril height distributions (right panel of Fig. 3) indicate that mean fibril heights decreased with increasing lignin content. The number-average heights were 13.4, 9.6 and 7.1 nm for CNF-BEP, LCNF-UHP-LL, and LCNF-UHP-HL, respectively. Furthermore, the distribution became narrower or more uniform as the lignin content increased. These results suggest that residual lignin promoted fibrillation, in agreement with a previous study (Rojo et al., 2015). Lignin, acting as an antioxidant, was suggested to stabilize cellulosic mechano-radicals formed during microfluidization (Solala et al., 2012). Cellulosic radicals are extremely reactive and could participate in recombination reactions to counteract fibrillation. Therefore, the radical scavenging ability of lignin led to less pronounced crosslinking of cellulose, easier defibrillation and more individualized nanofibrils (Rojo et al., 2015).

The presence of lignin, however, preserved fibril length, perhaps due to the fact that lignin protected excess cellulose depoly-

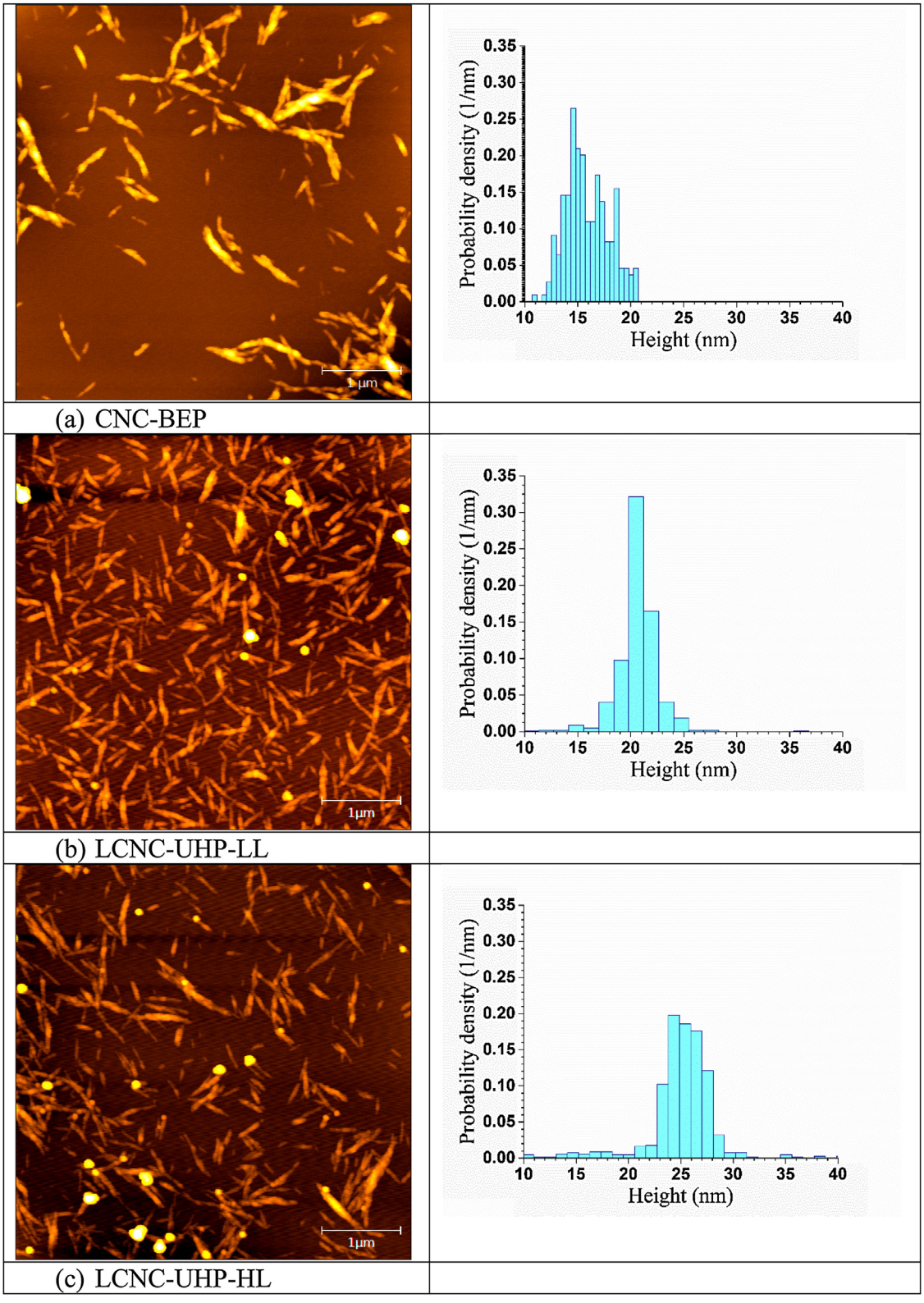

Fig. 2. AFM images of different lignocellulosic nanofibrils (LCNF) (left panel) from BEP (a), UHP-LL (b), and UHP-HL (c) and the corresponding height distribution measured from AFM topographic data (right panel). Scale = 1 μm.

merization by acid. AFM images show that CNF-BEP contains primarily short individual fibrils due to the strong hydrolysis severity (Fig. 3a), in agreement with our previous study using oxalic acid (Chen et al., 2016; Wang et al., 2017). Under the same hydrolysis severity, slightly longer fibrils were obtained from UHP-LL (Fig. 3b) than that from BEP (Fig. 3a). The light brown color of LCNF-UHP-LL sol indicated that the sample contains lignin. Much longer fibrils were obtained from UHP-HL (Fig. 3c). Lignin particles were visible

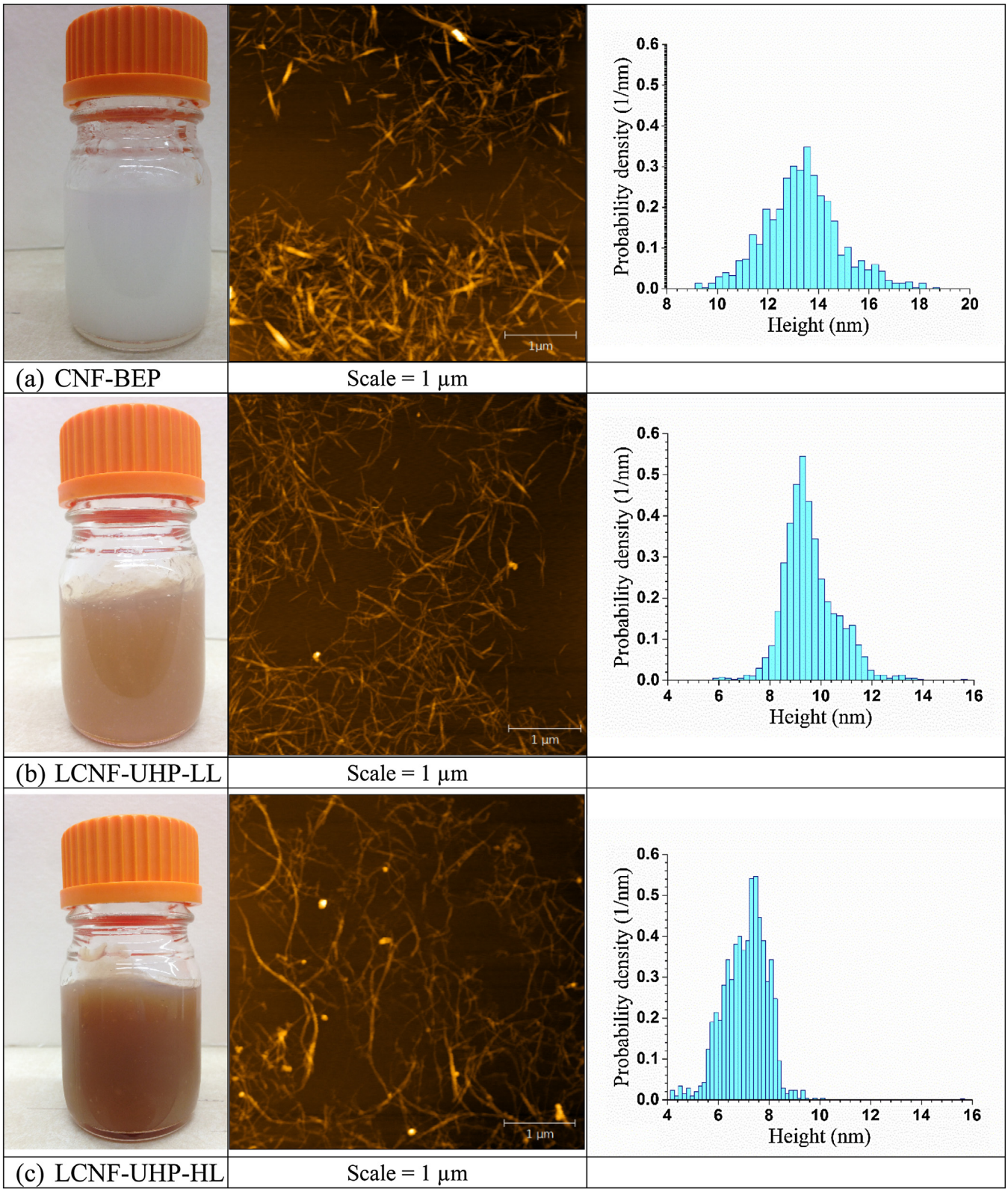

Fig. 3. Sol gel photos (left panel), AFM images (middle panel), and AFM measured height probability density distributions (right panel) of CNF-BEP (a), LCNF-UHP-LL (b), and LCNF-UHP-HL (c).

from the AFM images of the two LCNF from UHP. The (L)CNF mean lengths were visually estimated to be 350, 700, and 2000 nm based on the AFM images shown in Fig. 3, for CNF-BEP, LCNF-UHP-LL and LCNF-UHP-HL, respectively. As a result, the LCNF with higher lignin content had a much greater aspect ratio of approximately 280 based on the measured mean heights and estimated mean lengths which is beneficial for applications in polymer reinforcement.

3.3. Crystallinity

The crystallinity indices (CrI) of the original pulp fibers and their corresponding (L)CNF samples were measured using x-ray diffraction. The results (Table 2) indicate that acid hydrolysis with subsequent microfluidization resulted in a slight increase in CrI value for all three samples. Despite it is generally accepted that mechanical fibrillation may reduce cellulose crystallinity, acid hydrolysis dissolved a substantial amount of amorphous hemicelluloses (Qing et al., 2013; Wang et al., 2017), which resulted in the overall increase in measured sample crystallinity of the (L)CNF. Compared with the two LCNF, CNF-BEP had the highest CrI of 80.3%. This is most likely due to the presence of lignin in the two LCNF samples. The UHP-HL and LCNF-UHP-HL with the highest lignin content had the lowest CrI. Due to the low yields of LCNC with the limited amount of samples available, CrI measurement of the CNC-BEP and LCNC-UHP-LL and LCNC-UHP-HL were not carried out. It is expected that these samples should have higher CrI than their corresponding (L)CNF samples as demonstrated previously (Chen et al., 2016).

3.4. Carboxylation and dispersion stability

Fourier transform infrared (FTIR) spectroscopy was used to characterize the chemical structure of the lignocellulosic materials. As shown in Fig. 4, the absorption band at 1640 cm^{-1} was attributed to the vibration of water molecules, which was very difficult to extract due to the cellulose-water interaction (Adel, Abd El-Wahab, Ibrahim & Al-Shemy, 2011). The absorption bands at 1429, 1161 and 896 cm^{-1} in each sample are interpreted as typical cellulose structures (Leung et al., 2011; Schwanninger, Rodrigues, Pereira, & Hinterstoisser, 2004). The bands at 1507 and 1596 cm^{-1} are associated with the aromatic skeletal vibration of lignin (Schwanninger et al., 2004) and are only visible with the two UHP and their corresponding LCNF samples. A weak band was observed around 1722 cm^{-1} in the CNF-BEP and LCNF-UHP-LL samples that was not present in the feed fibers. This band corresponds to the C=O vibrations in the carbonyl group from cellulose esterification by maleic acid (Fischer & Speier, 1895); i.e., one of the carboxyl groups in the maleic acid reacted with cellulose to form ester groups on LCNF (Chen et al., 2016). However, the peaks at 1722 cm^{-1} were very weak, suggesting low to moderate esterification. The 1722 cm^{-1} peak is not observable from the LCNF-UHP-HL sample, indicating high lignin content may have prevented substantial cellulose esterification. Further study is needed in the future to differentiate the free carboxylic acid from the corresponding esters (1722 cm^{-1}) using counter ion exchange method (Hakalahti et al., 2016).

The qualitative FTIR features at 1722 cm^{-1} are consistent with the amounts of carboxyl groups measured by conductometric titration as shown in Table 2. The carboxyl group content in LCNF-UHP-HL was zero and were very low at <0.1 mmol/g for LCNF-UHP-LL and CNF-BEP. LCNC, however, are more carboxylated than LCNF, in agreement with our previous study using the same bleached eucalyptus pulp (Chen et al., 2016; Wang et al., 2017). Carboxyl group content for the two LCNC samples were above 0.2 mmol/g. The carboxyl group content of the two LCNC samples were lower than the CNC-BEP, again suggesting lignin may also play a barrier role in esterification cellulose.

Carboxylation can increase cellulose nanomaterial surface charge, or zeta potential, which should facilitate particle dispersion, a property that is important in the manufacturing products using cellulose nanomaterials. As expected, the measured fibril zeta potentials were proportional to carboxyl group content. To test dispersion stability versus zeta potential (or carboxyl group content), LCNF suspensions of 1 wt% were sonicated (Qsonica, LLC., Newtown, CT) in water at 25 °C for 5 min. Pictures of the sonicated

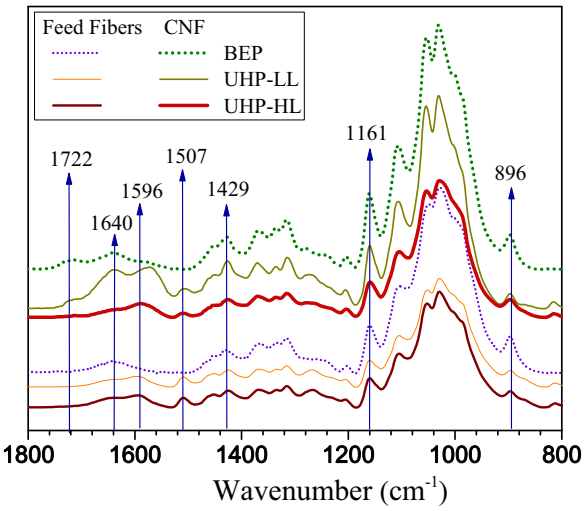

Fig. 4. FTIR spectra of BEP, UHP-LL, and UHP-HL fibers and their corresponding LCNF samples.

suspensions were taken during settling at 10 min, 2 h and 24 h. The stability of CNF-BEP and LCNF-UHP-LL was greater than that of the LCNF-UHP-HL whereby the fibrils of the latter settled in 4 h. The CNF-BEP and LCNF-UHP-LL did not settle completely even after 24 h. These results were primarily due to the surface charge difference among these three samples. Higher carboxyl group contents induced greater negative surface charges that impart electrostatic stabilization of the suspensions. LCNF-UHP-HL, however, had a non-detectable carboxyl groups and the lowest surface charge and therefore low suspension stability. The surface charge of the three (L)CNC samples were all greater than their corresponding (L)CNF samples (Table 2), suggesting these LCNC samples can form more stable colloidal suspensions than their corresponding LCNF suspensions.

3.5. Interaction with water

The water retention value (WRV) can be a measure of the interaction between a lignocellulosic material and water. Lignin containing pulp fibers have low WRV, as listed in Table 2, when compared to the bleached fibers. The higher the lignin content, the lower its WRV. For the two UHP samples, WRV dropped from 88 to 64, or approximately 27%, when lignin content increased from 3.9 to 17.2%. A similar decrease was also observed from their corresponding LCNF samples, i.e., WRV of LCNF decreased from 527 to 387, surprisingly also 27%. Lignin may be more or less uniformly distributed within the fibers after kraft pulping that has removed most of the lignin in the cell wall and middle lamella. As a result, nanofibrillation did not change the extent of the interaction between the resultant fibrils and water since the lignin is still evenly distributed. Compared with the CNF-BEP sample WRV of 1338, the WRV values of the two LCNF were substantially lower (Table 2) at 527 and 387, respectively. The decrease in WRV with the increase in lignin content is related to the hydrophobicity of lignin. From a molecular interaction point of view, undissolved lignin (inside cell wall) after pulping could control water contents and shield the free accessible hydroxyl group from the formation of hydrogen bonding with water molecules, resulting in the reduction of WRV (Spence, Venditti, Rojas et al., 2010). Another explanation, or co-factor is based on the porosity and voids created by the removal of lignin. Even though cellulose can imbibe large amount of water, the WRV also depends greatly on cracks, cavities and pores, which retain enormous amounts of water, which are also less prominent in less de-lignified fibers (Pejic, Kostic, Skundric, & Praskalo, 2008). Due to

limited amount of LCNC sample available, WRV were not measured; similar results, however, are expected.

3.6. Thermal stability

Thermogravimetric analyses were conducted to investigate the differences in thermal decomposition behavior and thermal stability of original fibers and LCNF samples (Adel et al., 2011). The weight loss curves and the derivative of the weight loss curves versus temperature (dW/dT) were obtained. The onset degradation temperature T_{onset}, defined as the temperature at which $dW/dT \geq 1$, and the maximal weight loss temperature T_{max} (Chancelier et al., 2014; Chen et al., 2016), defined as the temperature at which $|dW/dT|$ reached a maximum, were then determined (Table 2). Nanofibrillation substantially increased surface area of the fibrils resulting in reduced T_{max} when compared with their corresponding feed fibers (Quiévy et al., 2010). Lignin, as a complex three-dimensional polymer, is thermally more stable than cellulose and hemicelluloses (Brebu, Tamminen, & Spiridon, 2013). LCNF-UHP-HL with lignin content of 17.2% had the highest T_{max} of approximately 393 °C, compared with 361 °C for CNF-BEP, and 376 °C for LCNF-UHP-LL (lignin content of 3.9%). This indicates the advantages of using lignin containing cellulose nanomaterials for bio-composite applications. Due to limited amount of LCNC available, TGA analyses were not conducted. However, it is expected that LCNC samples, especially the one with high lignin content (LCNC-UHP-HL), should have very high thermal stability based on our previous study (Chen et al., 2016).

4. Conclusions

This study for the first time demonstrated integrated production of lignin containing and carboxylated LCNC along with LCNF using a fully recyclable di-carboxylic acid. LCNC yield was low, however, the market for LCNC is usually much smaller than LCNF. So the present process can meet the market demands for these two types of lignocellulosic nanomaterials. The ability to recycle acid and the substantially reduced energy input for mechanical fibrillation in producing LCNF make the solid di-carboxylic acid hydrolysis very promising to achieve low cost and sustainable and integrated production of thermally stable and carboxylated LCNC and LCNF.

Acknowledgements

This work was partially supported by US Forest Service, the Chinese State Forestry Administration (Project No. 2015-4-54), the National Natural Science Foundation of China (Project No. 31470599), the Doctorate Fellowship Foundation of Nanjing Forestry University. Funding from these programs made the visiting appointments of Bian at FPL possible. We also would like to acknowledge Dr. Goyal Gopal and their colleagues of International Paper Company for complimentarily providing us the unbleached mixed hardwood pulp samples.

Appendix A. Supplementary data

Supplementary data associated with this article can be found, in the online version, at http://dx.doi.org/10.1016/j.carbpol.2017.03.050.

References

Adel, A. M., Abd El-Wahab, Z. H., Ibrahim, A. A., & Al-Shemy, M. T. (2011). Characterization of microcrystalline cellulose prepared from lignocellulosic materials. Part II: Physicochemical properties. *Carbohydrate Polymers*, *83*(2), 676–687.

Allen, T. C., & Cuculo, J. A. (1973). Cellulose derivatives containing carboxylic acid groups. *Journal of Polymer Science: Macromolecular Reviews*, *7*, 189–262.

Brebu, M., Tamminen, T., & Spiridon, I. (2013). Thermal degradation of various lignins by TG-MS/FTIR and Py-GC–MS. *Journal of Analytical and Applied Pyrolysis*, *104*, 531–539.

Chancelier, L., Diallo, A. O., Santini, C. C., Marlair, G., Gutel, T., Mailley, S., et al. (2014). Targeting adequate thermal stability and fire safety in selecting ionic liquid-based electrolytes for energy storage. *Physical Chemistry Chemical Physics*, *16*(5), 1967–1976.

Chen, W. S., Yu, H. P., Liu, Y. X., Chen, P., Zhang, M. X., & Hai, Y. F. (2011). Individualization of cellulose nanofibers from wood using high-intensity ultrasonication combined with chemical pretreatments. *Carbohydrate Polymers*, *83*(4), 1804–1811.

Chen, L., Wang, Q., Hirth, K., Baez, C., Agarwal, U. P., & Zhu, J. Y. (2015). Tailoring the yield and characteristics of wood cellulose nanocrystals (CNC) using concentrated acid hydrolysis. *Cellulose*, *22*(3), 1753–1762.

Chen, L., Zhu, J. Y., Baez, C., Kitin, P., & Elder, T. (2016). Highly thermal-stable and functional cellulose nanocrystals and nanofibrils produced using fully recyclable organic acids. *Green Chemistry*, *18*, 3835–3843.

Eichhorn, S. J., Dufresne, A., Aranguren, M., Marcovich, N. E., Capadona, J. R., Rowan, S. J., et al. (2010). Review: Current international research into cellulose nanofibres and nanocomposites. *Journal of Materials Science*, *45*(1), 1–33.

Ferrer, A., Quintana, E., Filpponen, I., Solala, I., Vidal, T., Rodríguez, A., et al. (2012). Effect of residual lignin and heteropolysaccharides in nanofibrillar cellulose and nanopaper from wood fibers. *Cellulose*, *19*(6), 2179–2193.

Fischer, E., & Speier, A. (1895). Darstellung der Ester. *Chemische Berichte*, *28*, 3252–3258.

Hakalahti, M., Mautner, A., Johansson, L. S., Hänninen, T., Setälä, H., Kontturi, E., et al. (2016). Direct interfacial modification of nanocellulose films for thermoresponsive membrane templates. *ACS Applied Materials and Interfaces*, *8*(5), 2923–2927.

Hamad, W. Y., & Hu, T. Q. (2010). Structure–process–yield interrelations in nanocrystalline cellulose extraction. *Canadian Journal of Chemical Engineering*, *88*, 392–402.

Hoeger, I. C., Nair, S. S., Ragauskas, A. J., Deng, Y., Rojas, O. J., & Zhu, J. Y. (2013). Mechanical deconstruction of lignocellulose cell walls and their enzymatic saccharification. *Cellulose*, *20*(2), 807–818.

Iwamoto, S., Nakagaito, A. N., & Yano, H. (2007). Nano-fibrillation of pulp fibers for the processing of transparent nanocomposites. *Applied Physics A: Materials Science and Processing*, *89*, 461–466.

Leung, A. C., Hrapovic, S., Lam, E., Liu, Y., Male, K. B., Mahmoud, K. A., et al. (2011). Characteristics and properties of carboxylated cellulose nanocrystals prepared from a novel one-step procedure. *Small*, *7*(3), 302–305.

Li, P., Sirviö, A., Haapala, & Liimatainen, H. (2017). Cellulose nanofibrils from nonderivatizing urea-based deep eutecti solvent pretreatments. *ACS Applied Materials & Interfaces*, *9*, 2846–2855.

Liimatainen, H., Visanko, M., Sirviö, J. A., Hormi, O. E. O., & Niinimaki, J. (2012). Enhancement of the nanofibrillation of wood cellulose through sequential periodate-chlorite oxidation. *Biomacromolecules*, *13*(5), 1592–1597.

Luo, X., & Zhu, J. Y. (2011). Effects of drying-induced fiber hornification on enzymatic saccharification of lignocelluloses. *Enzyme and Microbial Technology*, *48*(1), 92–99.

Luo, X., Gleisner, R., Tian, S., Negron, J., Horn, E., Pan, X. J., et al. (2010). Evaluation of mountain beetle infested lodgepole pine for cellulosic ethanol production by SPORL pretreatment. *Industrial & Engineering Chemistry Research*, *49*(17), 8258–8266.

Pejic, B. M., Kostic, M. M., Skundric, P. D., & Praskalo, J. Z. (2008). The effects of hemicelluloses and lignin removal on water uptake behavior of hemp fibers. *Bioresource Technology*, *99*(15), 7152–7159.

Peyre, J., Pääkkönen, T., Reza, M., & Kontturi, E. (2015). Simultaneous preparation of cellulose nanocrystals and micron-sized porous colloidal particles of cellulose by TEMPO-mediated oxidation. *Green Chemistry*, *17*(2), 808–811.

Poletto, M., Zattera, A. J., Forte, M. M. C., & Santana, R. M. C. (2012). Thermal decomposition of wood: Influence of wood components and cellulose crystallite size. *Bioresource Technology*, *109*, 148–153.

Qin, Y., Qiu, X., & Zhu, J. Y. (2016). Understanding longitudinal wood fiber ultra-structure for producing cellulose nanofibrils using disk milling with dilute acid prehydrolysis. *Scientific Reports*, *6*, 35602.

Qing, Y., Sabo, R., Zhu, J. Y., Agarwal, U., Cai, Z., & Wu, Y. (2013). A comparative study of cellulose nanofibrils disintegrated via multiple processing approaches. *Carbohydrate Polymers*, *97*(1), 226–234.

Quiévy, N., Jacquet, N., Sclavons, M., Deroanne, C., Paquot, M., & Devaux, J. (2010). Influence of homogenization and drying on the thermal stability of microfibrillated cellulose. *Polymer Degradation and Stability*, *95*(3), 306–314.

Rojo, E., Peresin, M. S., Sampson, W. W., Hoeger, I. C., Vartiainen, J., Laine, J., et al. (2015). Comprehensive elucidation of the effect of residual lignin on the physical, barrier, mechanical and surface properties of nanocellulose films. *Green Chemistry*, *17*(3), 1853–1866.

SCAN. (2000). *SCAN-C 62:00 water retention value of chemical pulps*. Nordic Standardization Program.

Saito, T., Okita, Y., Nge, T. T., Sugiyama, J., & Isogai, A. (2006). TEMPO-mediated oxidation of native cellulose: Microscopic analysis of fibrous fractions in the oxidized products. *Carbohydrate Polymers*, *65*, 435–440.

Schwanninger, M., Rodrigues, J. C., Pereira, H., & Hinterstoisser, B. (2004). Effects of short-time vibratory ball milling on the shape of FT-IR spectra of wood and cellulose. *Vibrational Spectroscopy*, *36*(1), 23–40.

Segal, L., Creely, J. J., Martin, A. E., & Conrad, C. M. (1959). An empirical method for estimating the degree of crystallinity of native cellulose using the X-ray diffractometer. *Textile Research Journal*, *29*, 786–794.

Sehaqui, H., Kulasinski, K., Pfenninger, N., Zimmermann, T., & Tingaut, P. (2017). Highly carboxylated cellulose nanofibers via succinic anhydride esterification of wheat fibers and facile mechanical disintegration. *Biomacmolecules*, *18*(1), 242–248.

Siró, I., Plackett, D., Hedenqvist, M., Ankerfors, M., & Lindström, T. (2011). Highly transparent films from carboxymethylated microfibrillated cellulose: The effect of multiple homogenization steps on key properties. *Journal of Applied Polymer Science*, *119*(5), 2652–2660.

Solala, I., Volperts, A., Andersone, A., Dizhbite, T., Mironova-Ulmane, N., Vehniäinen, A., et al. (2012). Mechanoradical formation and its effects on birch kraft pulp during the preparation of nanofibrillated cellulose with Masuko refining. *Holzforschung*, *66*(4)

Spence, K. L., Venditti, R. A., Rojas, O. J., Habibi, Y., & Pawlak, J. J. (2011). A comparative study of energy consumption and physical properties of microfibrillated cellulose produced by different processing methods. *Cellulose*, *18*(4), 1097–1111.

Spence, K. L., Venditti, R. A., Habibi, Y., Rojas, O. J., & Pawlak, J. J. (2010). The effect of chemical composition on microfibrillar cellulose films from wood pulps: Mechanical processing and physical properties. *Bioresource Technology*, *101*(15), 5961–5968.

Spence, K. L., Venditti, R. A., Rojas, O. J., Habibi, Y., & Pawlak, J. J. (2010). The effect of chemical composition on microfibrillar cellulose films from wood pulps: Water interactions and physical properties for packaging applications. *Cellulose*, *17*(4), 835–848.

TAPPI. (1999). *TAPPI standard method (T236 om-99), Kappa number of pulp*. TAPPI.

Usov, I., Nyström, G., Adamcik, J., Handschin, S., Schütz, C., Fall, A., et al. (2015). Understanding nanocellulose chirality and structure-properties relationship at the single fibril level. *Nature Communications*, *6*, 7564. http://dx.doi.org/10.1038/ncomms8564

Wang, Q. Q., Zhu, J. Y., & Considine, J. M. (2013). Strong and optically transparent films prepared using cellulosic solid residue (CSR) recovered from cellulose nanocrystals (CNC) production waste stream. *ACS Applied Materials & Interfaces*, *5*(7), 2527–2534.

Wang, W. X., Mozuch, M. D., Sabo, R. C., Kersten, P., Zhu, J. Y., & Jin, Y. C. (2015). Production of cellulose nanofibrils from bleached eucalyptus fibers by hyperthermostable endoglucanase treatment and subsequent microfluidization. *Cellulose*, *22*(1), 351–361.

Wang, R., Chen, L., Zhu, J. Y., & Yang, R. (2017). Tailored and integrated production of carboxylated cellulose nanocrystals (CNC) with nanofibrils (CNF) through maleic acid hydrolysis. *ChemNanoMat*, *3* http://dx.doi.org/10.1002/cnma.201700015

Wang, Q. Q., Zhu, J. Y., Gleisner, R., Kuster, T. A., Baxa, U., & McNeil, S. E. (2012). Morphological development of cellulose fibrils of a bleached eucalyptus pulp by mechanical fibrillation. *Cellulose*, *19*(5), 1631–1643.

Wang, Q. Q., Zhu, J. Y., Reiner, R. S., Verrill, S. P., Baxa, U., & McNeil, S. E. (2012). Approaching zero cellulose loss in cellulose nanocrystal (CNC) production: Recovery and characterization of cellulosic solid residues (CSR) and CNC. *Cellulose*, *19*(6), 2033–2047.

Wang, Z. J., Zhu, J. Y., Zalesny, R. S. J., & Chen, K. F. (2012). Ethanol production form poplar wood the through enzymatic saccharification and fermentation by dilute acid and SPORL pretreatments. *Fuel*, *95*, 606–614.

Zhu, H., Luo, W., Ciesielski, P. N., Fang, Z., Zhu, J. Y., Henriksson, G., et al. (2016). Wood-derived materials for green electronics, biological devices, and energy applications. *Chemical Reviews*, *116*(16), 9305–9374.